INVESTIGATION OF "MCM-22", "ZSM-12 & 35 COMPOSITE", AND "ZEOLITE AL-MORDENITE & ZSM-39 COMPOSITE" CRYSTALS BY ANALYSIS OF CHARACTERIZATION TECHNIQUES

MINA KAMANI [a], MASOUMEHALSADAT RAHMATI [a], SAMIRA AMIRI KHOSHKAR VANDANI [a,b] AND GHAZALEH CHIZARI FARD [c,d]*

[a]*Department of Chemistry, South Tehran Branch, Islamic Azad University, Tehran, 11365-4435, Iran.*
[b]*Nanotechnology Research Center, South Tehran Branch, Islamic Azad University, Tehran, 11365-4435, Iran.*
[c]*Department of Biochemistry, School of Medicine, Iran University of Medical Sciences, Tehran, Iran.*
[d]*"Pajoohesh BAMA" Knowledge Enterprise Co & Clothing and Fabric Design Department, Art Faculty, Imam Javad University College, Yazd, Iran.*

ABSTRACT

Zeolites are three-dimensional, microporous, crystalline solids with well-defined structures that contain aluminum, silicon, and oxygen in their form. Cations and water are located in the pores of zeolites. They have a framework structure, in which interconnected cavities are occupied by large metal cations (positively charged ions), and water molecules. The formation of specific zeolites can occur by more than one crystallization pathway. Control in the crystallization pathway can lead to the formation of different species. In this study, two new zeolite nanocomposites were synthesized using fixed raw materials including solvent, reagent (which acts as a template in the formation of zeolite morphology), silica source, and sodium hydroxide alkali. "MCM-22" mesoporous was first synthesized and then a new morphology of "MCM-22" was synthesized by changing the temperature, time, and amount of water. Also, two nanocomposites "ZSM-12 & 35 Composite" and "Zeolite Al-mordenite & ZSM-39 Composite" were synthesized with very different properties in terms of surface to volume ratio, acidity, specific surface area, ratio of Si to Al, and three-dimensional crystal structure. Various characterization techniques were used to provide information to better understand the structural properties of crystalline zeolites. They were then characterized, and analyzed using X-Ray Diffraction (XRD), Field Emission Scanning Electron Microscopy (FESEM), Fourier-Transform Infrared Spectroscopy (FTIR), Energy-Dispersive X-ray Spectroscopy (EDS), Mapping, and BET/BJH (Brunauer-Emmett-Teller (BET) and Barret-Joyner-Halenda (BJH)) techniques. The results showed that the synthetic zeolites, despite having the same precursors, differed in terms of surface to volume ratio, acidity, specific surface area, Si/Al ratio, and three-dimensional crystal structure.

Keywords: Aluminosilicate, Catalyst, MCM-22, ZSM-12 & 35 Composite, Zeolite Al-mordenite & ZSM-39 Composite, Zeolite Crystallization.

1. INTRODUCTION

Many processes in different industries are performed through catalysts. Thus, the use of catalysts with mild conditions and low costs is very important [1]. Since homogeneous catalysts have the problem of separation in successive reactions, and heterogeneous catalysts have a lower level of contact between the catalyst and the reactant, the strategy of using porous solid catalysts was proposed. This series includes zeolite membranes and zeolites [2] (silicates or aluminum silicates, crystalline mesopores [3,4]), where tetrahedral aluminum and silicon atoms usually surround oxygen atoms. [5]), sulfated oxides such as TiO_2, SnO_2, and ZrO_2 [6,7], heteropoly acids [8], and sulfated carbon [9], which have been developed over the past decade. Porous solids, in which a large volume of the structure is formed by voids and cavities, have a high surface-to-volume ratio, great acidity property, high surface area/specific surface, three-dimensional crystalline structure with uniform nano-channels, high permeability, shape selectivity, high thermal/chemical stability, adjustable acidity, and high selectivity. Also, they have low corrosion and are easy to disassemble as heterogeneous catalysts [10-12]. Porous solids [13] are divided into 3 categories based on the radius of the cavities:

- Micropores (radius of cavities less than 2 nm, such as zeolites),
- Mesopores (radius of cavities between 2-50 nm, such as MCMs),
- Macropores (radius of cavities more than 50 nm) [14,15].

Unlike non-zeolite catalysts, the catalytic performance of zeolites depends not only on the acidity of the catalysts but also on the porous structure of the zeolites [16]. Today, more than 170 different zeolite structures have been reported to enable the engineering of pores and provide seemingly endless possibilities for adapting these materials to chemical reactions [17,18]. In some cases, mixed zeolites or composites are preferred because of their special performance. For example, the ZSM-5/ZSM-11 composite [19,20] showed high activity, selectivity, and good stability for the reaction of benzene alkylation with dilute ethylene as a mediator [20,21]. ZSM-5/Y composite consisting of a mechanical mixture of ZSM-5 and Y effectively catalyzed methanol conversion and aromatic alkylation [22,23]. Using Ag/CuO/MCM-48 catalyst, symmetric and asymmetric polyhydroquinoline derivatives with good properties as well as catalyst recycling ability were synthesized [24]. Recently, the synthesis of some microporous/mesoporous composites such as ZSM-5/MCM-41, Beta/MCM-41, Y/MCM-41, and Ti-Beta/SBA-15 has aroused much interest in catalytic applications as they can combine the benefits of using small materials with high activity plus the stability and scattered materials with large pores [25,26].

One of the most popular catalysts in the mesopore category is the MCM-22 from the MWW family, which is 2D and has separate channels [27]. A positive feature of two-dimensional zeolite structures is that each layer has holes layered on top of each other, making it easier to access the depth of the holes, as there is an empty space between the holes. [28]. The MCM-22 consists of two independent cavity systems, one formed by 2D sinusoidal channels, and the other by large super cages with an inner radius of 0.71 nm and an outer radius of 1.8 nm. Both systems are available through 10 MR (Member Rings). This cavity system has acidic properties. Undoubtedly, the acidic outer surface of zeolite MCM-22 plays an undeniable role in catalytic reactions [29,30].

ZSM zeolites, which belong to the pentasil family Framework Inverted (MFI-type), are very popular among scientists as petrochemical catalysts [31]. The ZSM-12 is a silica-rich zeolite composed of a one-dimensional 12-ring channel system and the openings of unique pores (6.1*5.7) A° [32]. As its pores are slightly larger than the ZSM-5, it can be a great choice for converting larger molecules that cannot easily penetrate the MFI (microfinance). Further, due to its acidic properties, it can be used as a useful catalyst in many reactions such as isomerization [33], hydroisomerization [34], and hydrocracking [35].

The ZSM-35 belongs to the FER topology, consisting of a two-dimensional intersection channel system, that is, the 10-member 10-channel ring channel 10 MR (0.42*0.54 nm) and the 8-member 8-channel ring channel 8 MR (0.35 nm), in parallel with the direction [001] and [010]. It is widely used in catalytic processes, such as the cracking of hydrocarbons, and the skeletal isomerization of n-olefins to iso-olefins [36,37].

ZSM-39 zeolite crystals (with MTN topology) from the Clathrasil family and analog silicate hydrate gas 17 A° [38], as with some other zeolites, can be used as adsorbents, optical materials, and especially advanced nonlinear optical materials [39], as well as catalysts [40-43]. The optical properties of ZSM-39 are due to the presence of heteroatoms [44] such as Ge and Al substituted in systems containing different amines [38,45-47]. Pure silica ZSM-39 zeolites consist of eight $5^{12}6^4$ packaged cages with a diameter of 7.44 A°, plus 8 packaged cages 5^{12} [45], and very narrow channels with a diameter of 2.61 A°, which are synthesized

*Corresponding author email: minakamani.mk@gmail.com

usually via methods such as hydrothermal [48-52], vapor phase transfer [53], as well as in non-aqueous conditions [50,54-56]. The structural features of the ZSM-39 make it capable of low absorption [55], but instead are very suitable for guest-host interactions [39].

High silica mordenite (MOR) zeolites are very popular because of their great thermal stability, high physical and chemical potentials, good chemical resistance, large pores, both Brønsted and Lewis acid sites, and high specific surface area [57]. This popular solid acid catalyst is considered one-dimensional for large molecules and has a two-dimensional molecular sieve for smaller molecules [58]. Mordenite properties include: a framework density of 17.2 T/1000 A˚, and Cmcm, (a = 18.3 A˚, b = 20.5 A˚, c = 7.5 A˚) [59,60]. Similar to chains in the MFI structure, pentasil units form chains containing oxygen bridges through the common edges. Mordenite grooved plates have 12-ring and 8-ring channels [61-63].

The catalytic performance of zeolites depends not only on the acidity of the catalysts but also on the porous structure of the zeolites. Thus, it is logical to conclude that the relationship between the structure and property of a zeolite is a key factor in productivity and selectivity for further improvement in catalyst performance [16]. Therefore, the identification of nucleation processes and crystallization of zeolites has been considered by many researchers and scientists [64]. Crystallographically, the formula of a zeolite cell unit can be shown as Eq. 1.

$$M_{x/n}\,[(AlO_2)_x\,(SiO_2)_y]\,w.H_2O \quad (1)$$

Where n is the capacity of the metal, w is the number of water molecules per unit cell, and x and y are the sum of the quadrilaterals in the unit cell. In most zeolites, the main building blocks, the four-sided AlO_4 and SiO_4, aggregate to form the Secondary Building Units (SBU); Which may be a few simple faces such as a cube, a hexagonal prism, or an octagonal cube. The zeolite structure consists of a collection of secondary units [64].

Zeolite membranes consist of two parts, a dense layer and a porous base. The porous base causes the mechanical strength of the membrane. The porous bases that are mainly used are ceramic and metal. Zeolite membranes can be synthesized on porous alumina bases, carbon materials, and porous glass. There are obstacles to understanding the crystallization of zeolites [64,65], including heterogeneity of the precursors [66], condensation steps leading to the aluminosilicate frameworks' formation, the existence of more than one path of crystallization in some cases and uncertainty about them, and disturbance of some techniques in the theory of crystallization [64,65].

For obtaining a clear perspective of crystallization process, we need a detailed information about various events which are taking part when the precursor particles transform from the amorphous phase to the complete crystal phase. One of the most common approaches for achieving this goal is a careful monitoring of various steps of crystallization process by using different characterization techniques in both molecular and micron scales [64]. In this method, for better understand the properties of the precursor and the final crystalline zeolite, different spectroscopy techniques such as MAS NMR, SAXS, XRD, SEM are using [67,68]. By analyzing the obtained results from these spectroscopic methods, it was understood that there are two main steps in the crystallization process. The first step in the crystal growth process, which occurs after the formation of viable nuclei, is the reorganization of amorphous aluminosilicate phase. Usually, this step takes place when the initial precursors are mixing. During this process, the bond angles of Si-O-Al related to the $Si(OAl)_4$ units are reorganized and create some crystals with rugged surface by operating on aggregates of the constant volume. In the second step, the crystallization process will be completed and the well shape zeolite will be produced. During the second step, the growth in crystallin system is governed by the solution-mediated transport which resulted to obtain higher quality crystals [64,69,70].

Accordingly, in this study, two new zeolite nanocomposites were synthesized using fixed raw materials including solvent, reagent (which acts as a template in the formation of zeolite morphology), silica source, and sodium hydroxide alkali. MCM-22 mesoporous zeolite was first synthesized by modifying the US patent method [71]. MCM-22 was then synthesized with a new morphology by changing the temperature, time, and amount of water. Also, two nanocomposites ZSM12 & 35 and ZSM-39 / Al mordenite with very different properties in terms of surface to volume ratio, acidity, specific surface area, ratio of Si to Al, and three-dimensional crystal structure were synthesized. Various characterization techniques were used to provide information to better understand the structural properties of crystalline zeolites.

2. EXPERIMENTS

2.1. Materials

Ammonium nitrate (NH_4NO_3), Hexamethyleneimine (HMI), Silicic acid (H_4O_4Si), Sodium aluminate ($NaAlO_2$), and sodium hydroxide (NaOH) were purchased from Merck Germany. All of the chemicals were used without further purification.

2.2.1. Synthesis of MCM-22

First Morphology: In a beaker and on a stirrer, 1.55g of NaOH was dissolved in 2ml of deionized water and then 1.87g of $NaAlO_2$ was added. Next, 13.5ml of HMI was added dropwise to the resulting mixture and rotated for 30min. After this period, 23.38g of silicic acid was slowly added to the mixture for at least 3h with 18ml of deionized water. The resulting relatively wet cake was moved into the autoclave and sealed well. The autoclave was placed on a heater stirrer at 45°C for 24h. After the end of the day, the autoclave was transferred to the oven at 150°C for 12 days. After this period, the hot autoclave was immediately plunged from the oven into a mixture of water and ice to cool. The product was filtered with centrifuge and deionized water and washed at least three times. The resulting precipitate was poured into a tile with a temperature tolerance of over 600°C and placed in the furnace according to the following temperature program as Table I.

Table 1. *Temperature Schedule Table for MCM-22(1st morphology).*

Step	Rate	Last temperature (°C)	Hold in the last temperature (h)
A	15	100	20
B	15	550	20
C	10	25	4

The solid was then refluxed twice in a row with 125ml NH_4NO_3 1M at 80°C for 6h. Between the two refluxes, the product was immediately washed once with centrifuge and deionized water. Upon completion of the second reflux, the product was allowed to remain in the acid for 12h without movement and temperature. It was then filtered with centrifuge and deionized water and washed at least three times. The resulting precipitate was poured onto a tile with a temperature tolerance of over 600°C and placed at room temperature for 24h and then placed in the furnace at 500°C for 4h. In the end, the product inside the oven was allowed to reach room temperature [29].

Second Morphology: In a beaker and on a stirrer, 1.55g of NaOH was dissolved in 2ml of deionized water and then 1.87g of $NaAlO_2$ was added. Next, 13.5ml of HMI was added dropwise to the resulting mixture and rotated for 30min. After this time, the beaker was transferred into a bath ultrasonic with 23.38g of silicic acid slowly added to the mixture for at least 3h with 78ml of deionized water. The resulting relatively wet cake was moved into the autoclave and sealed well. The autoclave was placed in the oven for 1.5 days at 45°C and 13.5 days at 150°C. Subsequently, the hot autoclave was immediately plunged from the oven into a mixture of water and ice for 1.5h to cool. The product was filtered with centrifuge and deionized water and washed at least three times. The resulting precipitate was poured onto a tile with a temperature tolerance of over 600°C and placed in the furnace according to the following temperature program as Table II.

Table 2. *Temperature Schedule Table for MCM-22(2nd morphology).*

Step	Rate (°C/min)	Last temperature (°C)	Hold in the last temperature (h)
A	15	120	24
B	15	25	2
C	15	550	24
D	4	25	4

After this timetable, the product was left in the oven for 1 day to cool. The solid was then refluxed twice in a row with 250ml 1M NH_4NO_3 at 80°C for 6h. Between the two refluxes, the product was immediately washed once with centrifuge and deionized water. Upon completion of the second reflux, the product was allowed to remain in the acid for 6h without movement and temperature. It was then filtered with centrifuge and deionized water and washed at least three times. The resulting precipitate was poured onto a tile with a temperature tolerance of over 600°C and placed at room temperature for 5 days and then placed in the furnace at 500°C for 4h. Eventually, the product inside the oven was allowed to reach room temperature [29].

2.2.2. Synthesis of ZSM-12 & ZSM-35 Composite

In a beaker and on a stirrer, 1.55g of NaOH was dissolved in 2ml of deionized water to which 1.87g of $NaAlO_2$ was then added. Next, 13.5ml of HMI was added dropwise to the resulting mixture and rotated for 30min. After this period, 23.38g of silicic acid was slowly added to the mixture for at least 5h with 78ml of deionized water. The resulting cake was moved into the autoclave and sealed well. The autoclave was placed on a heater stirrer for 2 days at 45°C. After the end of the day, the autoclave was transferred to the oven at 150°C for 12 days. After this period, the hot autoclave was immediately plunged from the oven into a mixture of water and ice to cool. The product was filtered with centrifuge and deionized water and washed at least three times. The resulting precipitate was poured onto a tile with a temperature tolerance of over 600 °C and placed in the furnace according to the following temperature program as Table III.

Table 3. *Temperature Schedule Table for ZSM-12 & ZSM-35 Composite.*

	Rate (°C/min)	Last temperature (°C)	Hold in the last temperature (h)
A	4	120	10
B	15	550	24
C	10	25	4

The product was allowed to reach room temperature in the off furnace. Then, the solid was refluxed twice in a row with 375ml NH_4NO_3 1M at 80°C for 6h. Between the two refluxes, the product was immediately washed once with centrifuge and deionized water. Upon completion of the second reflux, the product was allowed to remain in the acid for 12h without movement and temperature. It was then filtered with centrifuge and deionized water and washed at least three times. The resulting precipitate was poured onto a tile with a temperature tolerance of over 600°C and placed at room temperature for 4 days and then placed in the furnace at 500°C for 4h. Ultimately, the product inside the oven was allowed to reach room temperature [29,72].

2.2.3. Synthesis of Zeolite Al-mordenite & ZSM-39 Composite

In a beaker and on a stirrer, 1.55g of NaOH was dissolved in 2ml of deionized water and then 1.87g of $NaAlO_2$ was added. Subsequently, 13.5ml of HMI was added dropwise to the resulting mixture and rotated for 30min. After this period, 23.38g of silicic acid was slowly added to the mixture for at least 3h with 18ml of deionized water. The resulting relatively wet cake was moved into the autoclave and sealed well. The autoclave was placed on a heater stirrer at 45°C for 24h. After the end of the day, the autoclave was transferred to the oven at 150°C for 12 days. After this period, the hot autoclave was immediately plunged from the oven into a mixture of water and ice to cool. The product was filtered with centrifuge and deionized water and washed at least three times. The resulting precipitate was poured onto a tile with a temperature tolerance of over 600°C and placed in the furnace according to the following temperature program as in table IV.

Table 4. *Temperature schedule table for Zeolite Al-mordenite & ZSM-39 Composite.*

	Rate (°C/min)	Last temperature (°C)	Hold in the last temperature (h)
A	15	120	12
B	15	25	36
C	15	550	20

Once the timing was completed, the product reached room temperature at the off stove. The solid was then refluxed twice in a row with 400ml NH_4NO_3 2M at 80°C. The first reflux lasted 6h and the second reflux 4h, and there was no washing between the two refluxes. Upon completion of the second reflux, the product was allowed to remain in the acid for 1.5 days without movement and temperature. It was then filtered with centrifuge and deionized water and washed at least three times. The resulting precipitate was poured onto a tile with a temperature tolerance of over 600°C and exposed to room temperature for 3 days, and then placed in the furnace at 500°C for 4h. In the end, the product inside the oven was allowed to reach room temperature [32].

3. RESULTS AND DISCUSSION

3.1. XRD Analysis

XRD (Rigaku, Ultima IV) technique is a suitable method for evaluating the crystallinity of the synthesized crystal structure. The measured angle in this method ranged within 2-70° with a rate of 1°/min. The crystallinity phases of MCM-22 (1st & 2nd morphology), ZSM-12&35 Composite and Zeolite Al-mordenite & ZSM-39 Composite are shown in Figure 1 (a, b, and c) in order. The synthesized crystal structures were analyzed by XRD with Cu-Kα radiation (λ = 0.154 nm) operating at 40 kV and 30 mA. The crystallinity size of the aluminosilicates was obtained using Scherrer Eq. 2.

$$D = k \lambda / \beta \cos \theta \quad (2)$$

Where D denotes the mean of the crystalline dimension, k is the crystal constant (the X-ray wavelength corresponding to CuKα)[73] which is 0.89, θ represents the Bragg angle, λ is the wavelength of X, and β=FWHM (Full Width at Half Maximum) with radian unit for XRD desired peaks. The other method for obtaining the crystallinity size is the Williamson-Hall Eq. 3 [74,75]; where, unlike the Debye-Scherrer Equation that worked with the sharpest peak, 5-6 sharp peaks are used. Also, for its computation, the diffraction vector (K), Eq. 4, is first calculated, where ε is the strain. The mean size of the crystals and particles are well illustrated by XRD results (Figure 1) and FESEM images (Figure 2), respectively [76].

$$\beta \cos \theta / \lambda = k / D + (4\varepsilon) \times \sin \theta / \lambda \quad (3)$$
$$K = 2 \sin \theta / \lambda \quad (4)$$

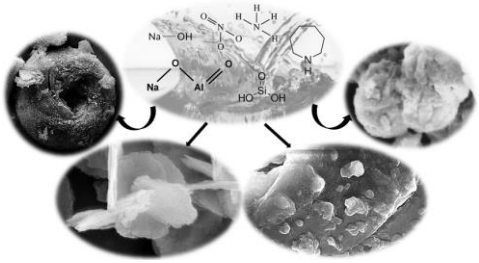

Figure 1. *Graphical abstract for this research.*

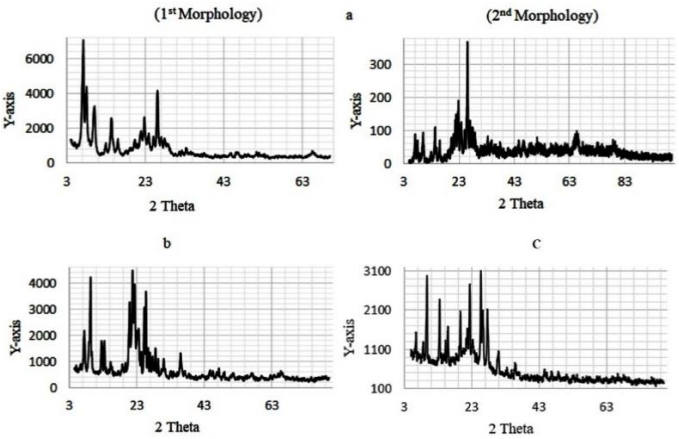

Figure 2. *XRD Analysis for a) MCM-22 (1st, & 2nd Morphology), b) ZSM-12 & 35 Composite, and c) Zeolite Al-mordenite & ZSM-39 Composite.*

The crystallinity in MCM-22 was determined based on its characteristic peaks [76], especially the peaks of the inner layer 7.1, 14.2, 25, and 26°, as well as the other two peaks at about 8 and 10°. The size of the MCM-22 crystals was

determined using the Debye-Scherrer model within 13.84-55.31 nm with the average crystallinity of the particles calculated to be about 30.51 nm.

In ZSM-12 & 35 Composite, the crystallinity was determined according to the sum of three intense reflections (2 θ = 9.2, 23.2, and 25.7°). Since the sharp peak for pure ZSM-35 is about 2θ=90° and the weaker peaks are around 23.2-25.7° [78,79] and the index peak for ZSM-12 is shared with ZSM-35 at about 23.2- 25.7° [80,81], it can confirm the possibility of simultaneous growth of both substances. This suggests that the synthesized ZSM-12&35 composite is not a separate crystal mechanical mixture from the ZSM-12 and ZSM-35, but maybe part of the growth of the ZSM-12 and ZSM-35 layers. The size of the ZSM-12 & 35 crystals was determined using the Debye-Scherrer model between 44.8-91.5 nm where the average crystallinity of the particles was calculated to be about 69.48 nm.

The crystallinity in Zeolite Al-mordenite & ZSM-39 composite was also determined by its index peaks (2θ = 6.4, 9.8, 13.3, 15.9, 22.5, 25.7, 26.3, and 27.8°). The index peaks for Zeolite Al-mordenite are in the range of 2θ = 13.5, 19.6, 22.3, 25.7, 26.3, 27.5, and 30.9° [40] and for ZSM-39, in the range of 2θ = 20-30° [41], which may confirm the simultaneous growth of both substances. This means that the synthesized Zeolite Al-mordenite & ZSM-39 composite is not a separate crystalline mechanical mixture from the ZSM-39 and Al-mordenite. The size of the Zeolite Al-mordenite & ZSM-39 composite crystals was determined using the Debye-Scherrer model between 22.44-89.79 nm with the average crystallinity of the particles calculated to be about 64.22 nm.

3.2. FESEM Analysis

The surface morphology of the samples was studied using FEI NOVANANOSEM 450 electron microscope.

Figure 2 a (1st & 2nd), b, and c displays the results obtained from the FESEM analysis of the synthesized structures. The overall shape of the particles can be deduced from the larger image by 10μm and the crystal plates from the image by 1μm.

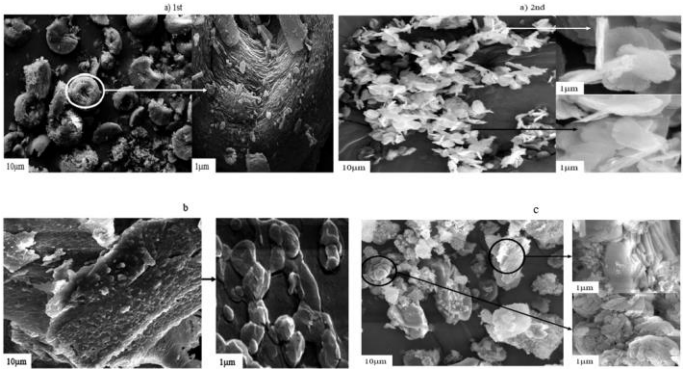

Figure 3. *FESEM Analysis for a) MCM-22 (1st, & 2nd Morphology), b) ZSM-12 & 35 Composite, and c) Zeolite Al-mordenite & ZSM-39 Composite.*

In the first morphology of MCM-22, the particles are layered and have platelet aggregation or donut-like platelets. In the second morphology, the particles are in the form of flowers or shells with layers stacked on top of each other.

The image of the oil droplets on the surface of the water seems similar to that of the ZSM-12 & 35 composite sample. Also, the size of the primary nanoparticles is 45-91 nm. Note that the additional absorption of organosilicon surfactants on the precursor levels of aluminosilicates can eventually lead to the destruction of the order of their structures [78].

According to Figure 2, it seems that the morphology of Zeolite Al-mordenite & ZSM-39 composite has a mix of spherical and pyramidal structure with the size of the primary nanoparticles between 147-180 nm.

3.3. FTIR Analysis

The vibrational pattern of the samples was determined using an FTIR spectrophotometer (Bruker, Tensor 27, and Equinox 55).

Figure 3 a, b, and c depict the FTIR spectra to describe functional groups and chemical bonds of MCM and the composites.

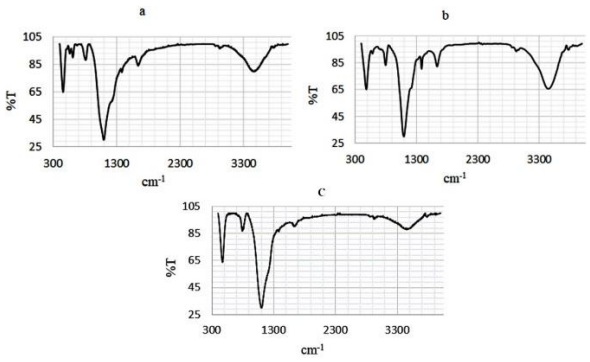

Figure 4. *FTIR Analysis for a) MCM-22, b) ZSM-12 & 35 Composite, and c) Zeolite Al-mordenite & ZSM-39 Composite.*

In the MCM-22 (1st morphology) sample, the presence of sharp peaks at 454.78, 560.25, 811.70, 1097.10, 1382.88, and 2926.60 cm^{-1} are related to Si-O-Si bending vibration, double ring, Si-O-Si (external asymmetric stretching), Si-O-Si (internal asymmetric stretching), Si-O-Si (external asymmetric stretching), and the silanol group, respectively [29]. Also, two strong adsorption bands can be seen at 3464.46 and 1639.00, which can be associated with the stretching vibration -OH of the absorbed water and the vibration of the Si-O-Si band, respectively [82,83].

In the case of ZSM-12 & 35 composite, the absorption peaks at 796.77, 1093.99, 1384.00, 1636.97, 2927.93, and 3456.31 cm^{-1} are related to Al-O bond, Si-O bonds, NO_3^- groups, the absorbed water during the synthesis process, the CH band, and the hydroxyl groups, respectively.

And finally, in the case of Zeolite Al-mordenite & ZSM-39 composite, the absorption peaks at 796.55, 1102.44, and 1639.18 cm^{-1} belong to the Al-O bond, Si-O bonds, water absorbed during the synthesis process, and so on. The absorption peak at 3456.21 cm^{-1} belongs to the hydroxyl groups. The adsorption peaks of the Al-O bond, and the Si-O bonds indicate the organization, and the frequency of the Si-O-Al bond angle in the crystal structure of the zeolites.

3.4. EDX, and Mapping Analysis

The elemental analysis of the nanocomposites was accomplished by an X-ray dispersive microanalyzer (Bruker, X Flash 6110).

EDX analysis was used to evaluate the chemical purity of the samples and to assess the percentage of available elements, while mapping analysis was applied to investigate how the elements were dispersed at the crystal lattice level, as shown in Figure 4 (a, b, and c). The data showed the presence of elements for MCM-22 and the composites.

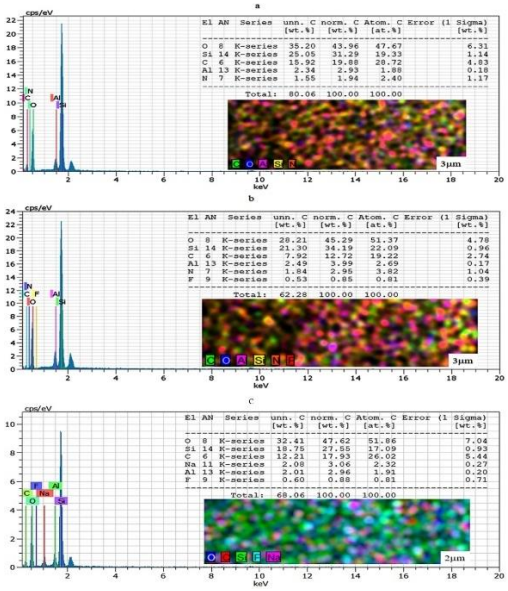

Figure 5. *EDX, and Mapping Analysis for a) MCM-22), b) ZSM-12 & 35 Composite and c) Zeolite Al-mordenite & ZSM-39 Composite.*

3.5. BET/BJH Analysis

The surface area of nanoparticles and nanocomposites was assessed using a BET analyzer (BELSORP Mini II). Also, the pore size distribution was studied using the BJH methodology concerning nitrogen adsorption/desorption isotherm. Figure 5 a, b, and c reveals the nitrogen adsorption/desorption isotherms of the samples.

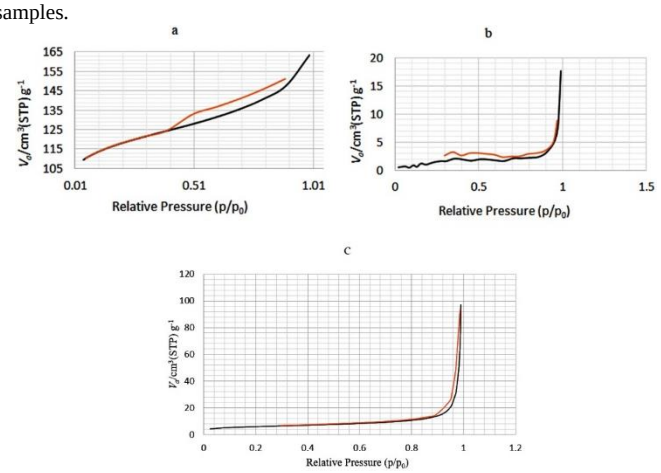

Figure 6. *BET/BJH Analysis for a) MCM-22), b) ZSM-12 & 35 Composite and c) Zeolite Al-mordenite & ZSM-39 Composite.*

The wall thicknesses of the samples were calculated based on Eq. 5.

Wall thickness = $(2d_{100} / \sqrt{3}) - D_{BJH}$ (5)

Where, $2d_{100}$ is 2θ with the Bragg angle, and D_{BJH} denotes the pore diameter obtained by the B_{JH} method (nm). The results of BET/BJH Analysis for a) MCM-22), b) ZSM-12 & 35 Composite and c) Zeolite Al-mordenite & ZSM-39 Composite are summarized in Table V.

After examining the isotherm for MCM-22 (1st morphology), it was observed that initially at a relative pressure of 0.5, an increase in adsorption occurred, which is related to the single-layer adsorption on the MWW surface. However, at relative pressures above 0.5 ($P / P_0 = 0.5$), nitrogen adsorption occurs in several layers, resulting in greater growth and gas adsorption near the standard relative pressure of $P / P_0 = 1$ and by increasing the adsorption and capillary density between MCM-22 particles and in large pores [84,85]. Based on the information obtained from the MCM-22 plot, and according to the IUPAC Classification, it was determined that the MCM-22 isotherm is a standard type IV isotherm and the hysteresis ring H1 is observed, which is usually characteristic of mesoporous materials [86].

The surface area of the ZSM-35 is 280.3 m^2 / g, while the surface area of the ZSM-12 is 487m^2/g, which is far larger than that of the ZSM-35. For ZSM-12 & 35 mechanical mixes, their BET levels appear to increase according to ZSM-12 content. Another factor influencing the increase in ZSM-12 & 35 levels is the fact that the adsorption of nitrogen molecules does not occur uniformly in one layer and takes place in irregular layers. This is because the layers are often completely filled before they begin to fill another layer. ZSM-12 & 35 isotherms of type IV with a hysteresis loop, which confirms the simultaneous presence of microporous and meso/macroporous in the ZSM-12&35 composite product. The synthesized sample isotherm showed a high absorption at low partial pressures of less than 0.1, suggesting the presence of micropores in the zeolite sample. On the other hand, the hysteresis loop in the region $0.45 < P / P0 < 0.95$ corresponds to a narrow or capillary density in the mesoporous material [87,88].

As shown in Figure 5, Zeolite Al-mordenite & ZSM-39 Composite has a diameter, pores, and adsorption volume matching the result obtained by XRD. The absorption isotherm observed at a low relative pressure ($P / Po < 0.01$), according to all zeolites, indicates the presence of micropores. For low relative pressures, a slow absorption has taken place. This behavior can be interpreted by the fact that zeolites are filling the microporous of their structure and proving the existence of microporous.

For high pressures, rapid adsorption occurs, indicating the presence of voids in the crystalline structure of the zeolite. In addition, the formed zeolites show a hysteresis loop at relative pressures above 0.4 ($0.4<P/P0<0.95$) due to the presence of mesoporous channels. The data show a typical IV absorption isotherm with the hysteresis ring H3, which corresponds to the IUPAC classification [87,88].

Table 5. *BET/BJH Parameters of the Synthesized MCM-22, ZSM-12&35 Composite, and Zeolite Al-mordenite & ZSM-39 Composite.*

Sample	S_{BET} m^2/g	Pore diameter by B_{JH} method (nm)	Total pore volume (p/p_0=0.990) cm^3/g	Wall thickness diameter (nm)
MCM-22	398.336	1.30	1.303	7.014
ZSM-12&35 Composite	7.5197	1.21	0.026922	2.920
Zeolite Al-mordenite & ZSM-39 Composite	20.878	1.21	0.141	6.343

3.6. Discussion

As mentioned earlier, many processes in various industries are performed with the help of zeolites, because of their properties include high surface to volume ratio, excellent and adjustable acidity, high surface area / specific surface, three-dimensional crystal structure with uniform nanochannels, high permeability, shape selectivity, high temperature/chemical stability, high selectivity, low corrosion, and porous structure. The catalytic performance of zeolites depends especially on factors such as catalytic acidity and their porous structure. Temperature, time, molar compound, pH, silica, alumina source, and surfactant are effective in the synthesis of zeolites [89-91].

Experimental results show that the first stage of crystallization occurs by organizing amorphous aluminosilicate units during the mixing of precursors. In the studied system, the crystallization process can be divided into two stages during which the crystallization process is controlled by different crystallization mechanisms. After the formation of living nuclei, the first stage of the crystal growth process continues with the new formation of a uniform, amorphous aluminosilicate phase that forms during the mixing of the primary precursors. This new configuration involves sorting the Si-O-Al bonding angle from the main constituent units, $Si(OAl)_4$ [92-94]. The formation steps of zeolites are done according to the following chemical equation:

$$NaOH(aq) + NaAl(OH)_4\ (aq) + Na_2\ SiO_3\ (aq) \dashrightarrow [Na_a\ (AlO_2)\ b\ (SiO_2)\ c.\ NaOH.\ H_2O]\ (gel) \dashrightarrow Na_x\ [(AlO_2)_x\ (SiO_2)_y].\ mH_2O$$

Although the amount and type of solvent are some of the important factors in molecular changes, this study was done without any change in the solvent [95-99]. In this study, the MCM-22 catalyst was synthesized by modifying the US patent method [71]. Then the effect of temperature, time, and amount of water on catalysts was investigated. The source of silica and sodium hydroxide was kept constant in all tests. By changing the temperature conditions, increasing the amount of water, and aging MCM-22 was synthesized with a new morphology. In all conditions, the process of synthesizing the 3rd and 4rd catalysts are the same as the synthesis of the second stage except for time and the amount of water, which led to the production of the new "ZSM-12&35 Composite", and "Zeolite Al-mordenite & ZSM-39 Composite". The crystallographic results of the XRD analysis and summary of parameter changes during synthesis are given in Tables VI and VII, respectively.

Table 6. *A Summary of the Synthesis Results from the XRD Analysis.*

Compound Name	Chemical Formula	Subfiles and quality	Primary reference
Zeolite MCM-22	$Al_2\ O_3$ .21 $Si\ O_2$	Inorganic Zeolite Low precision (O)	Bundens, R., Keville, K., Huss, Jr., A., Chu, C., Husain, A., 5,146,029., U.S. Patent, (1992)
ZSM-12	$Na_{1.16}Al_2\ Si_{77.4}O_{158.38}$	Inorganic Zeolite	Rosinski, E., Rubin, M., 3,832,449., U.S. Patent, (1974)
ZSM-35	$Na_{0.22}Al_2\ Si_{29.9}O_{64.45} \cdot 9.9H_2O$	Corrosion Inorganic Mineral Zeolite Low precision (O)	Plank, C., Rosinski, E., Rubin, M., 4,081,490., U.S. Patent, (1978)
ZSM-39	SiO_2	Alloy, metal or intermetalic Inorganic Zeolite Low precision (O)	Dwyer, F., Jenkins, E., 4,357,233., U.S. Patent, (1982)
Zeolite Al-mordenite	$Na_2\ Al_2\ Si_{13.3}O_{29.6+x}$	Inorganic Mineral Zeolite	Chandwadkar, A., Abdulla, R., Hegde, S., B-Nagy, J., Zeolites, 13, 470, (1993)

Table 7. *Summary of Parameters Comparing in the Synthesis Processes.*

Silica Source	H_2O (ml)	Temperature Program	Aging (day)	Chemical Formula	Nanocatalyst
Silicic Acid	20	As Table I	13	$Na_{1.16}\ Al_2\ Si_{77.4}\ O_{158.38}$	MCM-22 (donut-like platelets)
Silicic Acid	80	As Table II	15	$Na_{92}\ Al_{92}\ Si_{100}\ O_{384}$	MCM-22 (shells)
Silicic Acid	80	As Table III	14	$H_{2.37}Na_{3.10}(Al_{0.36}B_{5.11}Si_{66.53})O_{144}$ and $Na_{1.16}Al_2\ Si_{77.4}O_{158.38}$	ZSM-12&35 Composite
Silicic Acid	20	As Table IV	13	$Na_2\ Al_2\ Si_{13.3}\ O_{29.6+x}$ and $Si\ O_2$	Zeolite Al-mordenite & ZSM-39 Composite

CONCLUSIONS

Considering the application of zeolites in today's life and the necessity of using them in different industries, the synthesis and characterization of 3 types of functional zeolites were studied in this study. First, MCM-22 with first morphology was synthesized by modifying the patent US5362697A [1] and using the same precursor in that patent. Then, three more zeolites were synthesized using the same precursor and changing only three agents: one was the second morphology of zeolite MCM-22, then zeolite ZSM-12 & 35 composite, and the other was zeolite Al-mordenite and ZSM-39 Composite. The synthesized zeolites were then characterized. The results of characterization analyses showed the existence of the second morphology of zeolite MCM-22. These results also confirmed the simultaneous growth of both substances ZSM-12 and ZSM-35 in ZSM-12 & 35 composite; and the simultaneous growth of both substances ZSM-39 and Zeolite Al-mordenite in Zeolite Al-mordenite & ZSM-39 Composite. Comparing the results of the XRD model with the EDX results, it was proved that the Si / Al ratio in all cases is about 1 with a very small value, which is completely consistent with the definition of this ratio for zeolites. The total volume of cavities and the specific surface area of MCM-22 zeolite were significantly larger than other synthetic composites.

ACKNOWLEDGMENTS

The authors would like to thank Dr. Reza Fazaeli for his advice.

DECLARATIONS

Funding: This research has been done with personal funding and at the Nanotechnology Research Center, Islamic Azad University, South Tehran Branch.

CONFLICTS OF INTEREST

The authors declare that there is no conflict of interest.

AUTHOR'S CONTRIBUTIONS

All authors contributed equally to this work.

REFERENCES

1. M. S. Seyedi, M. Bahmaei, A. Farshi, Orient. J. Chem 31, 2409, (2015).
2. C. R. Patil, P. S. Niphadkar, V. V. Bokade, P. N. Joshi, Catal. Commun. 43, 188, (2014).
3. Z. S. Lin, D. Chen, H. Y. Nie, Y. A. Wong, Y. Huang, Can. J. Chem 97, 840, (2019).
4. 4. M. A. Camblor, S. Bong Hong, J. Porous Mater.265, (2010).
5. H. M. Lankapati, D. R. Lathiya, L. Choudhary, A. K. Dalai, K. C. Maheria, ChemistrySelect 5, 1193, (2020).
6. H. E. Hoydonckx, D. E. De Vos, S. A. Chavan, P. A. Jacobs, Top Catal 27, 83, (2004).
7. J. L. Ropero-Vega, A. Aldana-Pérez, R. Gómez, M. E. Niño-Gómez, APPL CATAL A-GEN 379, 24, (2010).
8. Y. Chen, X. Zhang, M. Dong, Y. Wu, G. Zheng, J. Huang, X. Zheng, J Taiwan Inst Chem Eng 61, 147, (2016).
9. F. D. Pileidis, M. Tabassum, S. Coutts, M. M. Titirici, Chinese J. Catal 35, 929, (2014).
10. U. Laska, C. G. Frost, G. J. Price, P. K. Plucinski, J. Catal. 268, 318, (2009).
11. R.M. Barrer, W.M. Meier, Trans. Faraday Soc. 54, 1074, (1958).
12. Y. Posada, AIP, 126108, (2009).
13. A. V. Agafonov, E. P. Grishina, Russ. J. Inorg 64, 1641, (2019).
14. P. T. Anastas, M. M. Kirchhoff, T. C. Williamson, APPL CATAL A-GEN 221, 3, (2001).
15. E. I. Negishi, L. Anastasia, Chem. Rev. 103, 1979, (2003).
16. J. Pérez-Ramírez, C. H. Christensen, K. Egeblad, C. H. Christensen, J. C. Groen, Chem. Soc. Rev. 37, 2530, (2008).
17. S. Amiri Khoshkar Vandani, R. Fazaeli, M. Giahi Saravani, H. Pasdar, Egypt. J. Chem., (2021).
18. L. B. McCusker, C. Baerlocher, D. Olson, Atlas of zeolite framework types. Elsevier sci., (2007).
19. Q. Wang, S. Zhang, G. Cai, F. Li, L. Xu, Z. Huang, Y. Li, U.S. Patent No. 6,093,866. Washington, DC: U.S. Patent and Trademark Office, (2000).
20. G. T. Kokotailo, US 4,229,424, (1980).
21. G. T. Kokotailo, US 4,289,607, (1981).
22. I. P. Dzikh, J. M. Lopes, F. Lemos, F. R. Ribeiro, APPL CATAL A-GEN 176, 239, (1999).
23. I. P. Dzikh, J. M. Lopes, F. Lemos, F. R. Ribeiro, Catal. Today 65, 143, (2001).
24. N., Bazdid-Vahdaty, M., Mamaghani, B., Khalili, F. Tavakoli, J. Chil. Chem. Soc 66, 5136, (2021).
25. Y. Han, F. S. Xiao, Chinese J. Catal 24, 149, (2003).
26. M. Rahmati, R. Fazaeli, M. G. Saravani, R. Ghiasi, Phys. Chem. Res. 8, 585, (2020).
27. V. A. Ostroumova, A. L. Maksimov, Pet. Chem. 59, 788, (2019).
28. S. L. Lawton, M. E. Leonowicz, R. D. Partridge, P. Chu, M. K. Rubin, MICROPOR MESOPOR MAT 23, 109, (1998).
29. H. Hoseini, M. Gorjizadeh, S. Sayyahi, K. A. SHAHBAZI, 131, (2017).
30. A. Corma, U. Diaz, V. Fornés, J. M. Guil, J. Martinez-Triguero, E. J. Creyghton, J. Catal. 191, 218, (2000).
31. L. L. Korobitsyna, L. M. Velichkina, A. V. Vosmerikov, V. I. Radomskaya, E. S. Astapova, N. V. Ryabova, O. A. Agapyatova, Russ. J. Inorg 53, 169, (2008).
32. X. Wei, P. G. Smirniotis, MICROPOR MESOPOR MAT 89, 170, (2006).
33. J. A. Martens, J. Perez-Pariente, E. Sastre, A. Corma, P. A. Jacobs, Appl. Catal. 45, 85, (1988).
34. S. Mehla, K. R. Krishnamurthy, B. Viswanathan, M. John, Y. Niwate, K. Kumar, B. L. Newalkar, J. Porous Mater 20, 1023, (2013).
35. W. Zhang, P. G. Smirniotis, J. Catal. 182, 400, (1999).
36. I. Rahmin, A. Huss Jr, D. N. Lissy, D. J. Klocke, W. O. Haag, U.S. Patent No. 5,449,851. Washington, DC: U.S. Patent and Trademark Office, (1995).
37. Z. Wu, Q. Wang, L. Xu, S. Xie, Stud Surf Sci Catal142, 747, (2002).
38. J. L. Schlenker, F. G. Dwyer, E. E. Jenkins, W. J. Rohrbaugh, G. T. Kokotailo, W. M. Meier, Nature 294, 340, (1981).
39. C. Xue, T. Xu, Mater. Lett. 112, 200, (2013).
40. A. Corma, Chem. Rev. 97, 2373, (1997).
41. A. Mech, A. Monguzzi, F. Meinardi, J. Mezyk, G. Macchi, R. Tubino, J Am Chem Soc 132, 4574, (2010).
42. Y. Wang, H. Li, L. Gu, Q. Gan, Y. Li, G. Calzaferri, MICROPOR MESOPOR MAT 121, 1, (2009).
43. Y. Ding, Y. Wang, H. Li, Z. Duan, H. Zhang, Y. Zheng, J. Mater. Chem. 21, 14755, (2011).
44. R. B. Borade, Zeolites 7, 398, (1987).
45. A. Huang, J. Caro, J. Cryst. Growth 311, 4570, (2009).
46. U. Deforth, K. K. Unger, F. Schüth, Microporous MAT 9, 287, (1997).
47. H. Sasaki, H. Jon, M. Itakura, T. Inoue, T. Ikeda, Y. Oumi, T. Sano, J. Porous Mater 16, 465, (2009).
48. X. Tang, Y. Sun, T. Wu, L. Wang, L. Fei, Y. Long, J. Chem. Soc. Faraday Trans. 89, 1839, (1993).
49. H. Gies, F. Liebau, H. Gerke, Angewandte Chemie International Edition in English 21, 206, (1982).
50. Y. Long, H. He, P. Zheng, G. Wu, B. Wang, J. Incl. Phenom. 5, 355, (1987).
51. J. J. Seral, S. Uriel, J. Coronas, Wiley, (2008).
52. M. Song, X. Wang, W. Zhou, H. He, Y. Sun, T. Wu, Y. Long, J. Solid State Chem 164, 19, (2002).
53. J. Dong, X. Tong, J. Yu, H. Xu, L. Liu, J. Li, Mater. Lett. 62, 4, (2008).
54. D. M. Bibby, L. M. Parker, Zeolites 3, 11, (1983).

55. B. Marler, N. Dehnbostel, H. H. Eulert, H. Gies, F. Liebau, J. Incl. Phenom. 4, 339, (1986).
56. Z. A. Lethbridge, D. S. Keeble, D. Walker, P. A. Thomas, R. I. Walton, J. Appl. Crystallogr. 43, 168, (2010).
57. A. N. Van Laak, S. L. Sagala, J. Zečević, H. Friedrich, P. E. De Jongh, K. P. De Jong, x J. Catal. 276, 170, (2010).
58. E. M. Flanigen, Stud Surf Sci Catal 137, 11, (2001).
59. S. Narayanan, P. Tamizhdurai, V. L. Mangesh, C. Ragupathi, A. Ramesh, RSC Advances 11, 250, (2021).
60. C. Perego, R. Millini, Chem. Soc. Rev. 42, 3956, (2013).
61. Z. Ma, J. Xie, J. Zhang, W. Zhang, Y. Zhou, J. Wang, MICROPOR MESOPOR MAT 224, 17, (2016).
62. S. K. Wahono, A. Suwanto, D. J. Prasetyo, T. H. Jatmiko, K. Vasilev, Appl. Surf. Sci 483, 940, (2019).
63. L. B. McCusker, C. Baerlocher, Introduction to Zeolite science and practice 168, 13, (2007).
64. M. Smaihi, O. Barida, V. Valtchev, EurJIC 2003, 4370, (2003).
65. K. N. Bozhilov, T. T. Le, Z. Qin, T. Terlier, A. Palčić, J. D. Rimer, V. Valtchev, Sci. Adv. 7, eabg0454, (2021).
66. G., Harvey, L. S. Dent Glasser, (1989).
67. P. Singh, T. Dowling, J. Watson, J. White, Phys. Chem. 1, 4125, (1999).
68. J. Shi, M. W. Anderson, S. W. Carr, Chem. Mater. 8, 369, (1996).
69. P. P. E. de Moor, T. P. Beelen, R. A. van Santen, Microporous MAT 9, 117, (1997).
70. X. Li, K. Li, H. Ma, R. Xu, S. Tao, Z. Tian, MICROPOR MESOPOR MAT 217, 54, (2015).
71. A. S. Fung, S. L. Lawton, W. J. Roth, U.S. Patent No. 5,362,697, (1994).
72. R. Mokaya, ChemPhysChem 3, 360, (2002).
73. R. Fazaeli, N. E. Fard, Russ. J. Appl. Chem 93, 973, (2020).
74. D. Nath, F. Singh, R. Das, MATER CHEM PHYS 239, 122021, (2020).
75. M. Kamani, R. Fazaeli, M. Arjmand, M. Ghorbani, Phys. Chem. Res. 8, 175, (2020).
76. L., Nassaji-Jahromi, R., Fazaeli, R., Behjatmanesh-Ardakani, M. Taghdiri, J. Chil. Chem. Soc 65, 5027, (2020).
77. B. Gil, W. J. Roth, J. Grzybek, A. Korzeniowska, Z. Olejniczak, M. Eliáš, J. Čejka, Catal. Today 304, 22, (2018).
78. 78. X. Niu, Y. Song, S. Xie, S. Liu, Q. Wang, L. Xu, Catal. Lett. 103, 211, (2005).
79. O. Igbari, Y. Xie, Z. Jin, L. S. Liao, J. Alloys Compd. 653, 219, (2015).
80. P. Dugkhuntod, T. Imyen, W. Wannapakdee, T. Yutthalekha, S. Salakhum, C. Wattanakit, RSC advances 9, 18087, (2019).
81. S. Kim, S. Philippot, S. Fontanay, R. E. Duval, E. Lamouroux, N. Canilho, A. Pasc, RSC advances 5, 90550, (2015).
82. J. Si, L. Li, Y. Zhang, J. C. Zhou, W. Ouyang, MRC 6, 15, (2017).
83. J. Zhou, X. Yang, Y. Wang, W. Chen, Catal. Commun. 46, 228, (2014).
84. N. E. Fard, R. Fazaeli, M. Yousefi, S. Abdolmohammadi, Appl. Phys. A 125, 1, (2019).
85. N. E. Fard, R. Fazaeli, M. Yousefi, S. Abdolmohammadi, Chem. Select 4, 9529, (2019).
86. D. Pérez-Quintanilla, I. Del Hierro, M. Fajardo, I. Sierra, J. Hazard. Mater. 134, 245, (2006).
87. G. Tang, M. Li, B. Wang, Y. Fang, T. Tan, MICROPOR MESOPOR MAT 265, 172, (2018).
88. M. A. Klunk, S. B. Schröpfer, S. Dasgupta, M. Das, N. R. Caetano, A. N. Impiombato, C. A. M. Moraes, Chem. Papers, 1, (2020).
89. 89 M. Kamani, R. Fazaeli, M. Arjmand, M. Hossein Ghorbani, J. Chil. Chem. Soc 65, 4833, (2020).
90. S. A. K. Vandani, R. Fazaeli, M. G. Saravani, H. Pasdar, J. Environ. Eng. Sci. 40, 1, (2021).
91. M. S. Rahmati, R. Fazaeli, M. G. Saravani, R. Ghiasi, J Nanostruct, 1, (2021).
92. M. Khanmoradi, M. Nikoorazm, A. Ghorbani-Choghamarani, Appl 31, e3693, (2017).
93. I. Mochida, S. Eguchi, M. Hironaka, S. I. Nagao, K. Sakanishi, D. D. Whitehurst, Zeolites 18, 142, (1997).
94. W. M. Meier, D. H. Olson, C. Baerlocher, Zeolites 17, (1996).
95. P. Selvarengan, P. Kolandaivel, Journal of Molecular Structure: THEOCHEM 617, 99, (2002).
96. S. B. Allin, T. M. Leslie, R. S. Lumpkin, Chem. Mater. 8, 428, (1996).
97. A. J. Aquino, D. Tunega, G. Haberhauer, M. H. Gerzabek, H. Lischka, J. Phys. Chem. A 106, 1862, (2002).
98. T. S. Vishkaee, R. Fazaeli, M. Yousefi, Russ. J. Inorg 64, 237, (2019).
99. M. Iranpour, R. Fazaeli, M. S. Sadjadi, M. Yousefi, Russ. J. Inorg 63, 1079, (2018).